Journal of Hydrology: Regional Studies 26 (2019) 100630

Contents lists available at ScienceDirect

Journal of Hydrology: Regional Studies

journal homepage: www.elsevier.com/locate/ejrh

Investigating the use of satellite-based precipitation products for monitoring water quality in the Occoquan Watershed

Jennifer Solakian[a,*], Viviana Maggioni[a], Adnan Lodhi[b], Adil Godrej[b]

[a] Department of Civil, Environmental and Infrastructure Engineering, George Mason University, 4400 University Drive, MS 6C1, Fairfax, Virginia, USA
[b] Occoquan Watershed Monitoring Laboratory, Department of Civil and Environmental Engineering, Virginia Tech, 9408 Prince William Street, Manassas, Virginia, USA

ARTICLE INFO

Keywords:
Satellite-based precipitation
Hydrologic modeling
Water quality simulations
Occoquan Watershed
TMPA
PERSIANN
CMORPH

ABSTRACT

Study Region: The Washington D.C area.
Study Focus: This work investigates the potential of using satellite-based precipitation products in a hydrological model to estimate water quality indicators in the Occoquan Watershed, located in the suburban Washington D.C area. Three (3) satellite-based precipitation products based on different retrieval algorithms (the Tropical Rainfall Measuring Mission Multi-satellite Precipitation Analysis, TMPA 3B42-V7; the Climate Prediction Center's CMORPH product; and the Precipitation Estimation from Remotely Sensed Information using Artificial Neural Networks Cloud Classification System, PERSIANN−CCS) are compared to gauge-based records over a 5-year period across the study region. The 3 satellite-based precipitation products and the gauge-based dataset are used as input to the Hydrologic Simulation Program FORTRAN (HSPF) hydrology and water quality model. Each satellite precipitation-forced simulation is compared to the reference model simulation forced with the gauge-based observations, in terms of streamflow and water quality indicators, i.e., stream temperature (TW), total suspended solids (TSS), dissolved oxygen (DO), and biological oxygen demand (BOD).
New Hydrological Insights for the Region: Results indicate that the spatiotemporal variability observed in the satellite-based precipitation products has a quantifiable impact on both modeled streamflow and water quality indicators. All 3 satellite products present moderate agreements with the reference precipitation and simulation; CMORPH presenting the best overall performance followed closely by TMPA, and PERSIANN presenting a comparatively inferior performance in terms of correlation, root-mean-square error and bias for streamflow and water quality indicators, such as TW, TSS, DO and BOD concentrations.

1. Introduction

The performance of both lumped and distributed hydrologic models is significantly influenced by a number of factors that contribute to uncertainty, e.g., observation errors, boundary or initial conditions errors, model or system errors, scale discrepancies, and unknown heterogeneity of parameters. Nevertheless, precipitation is widely accepted as the most influential meteorological input in hydrological and water quality investigations. Reliable and consistent hydrologic predictions for water quantity and quality depend on the accurate measurement of precipitation. The accuracy of precipitation data, including its intensity, duration, spatial patterns, and extent greatly influences the output of land surface and hydrologic models (Maggioni et al., 2013; Sorooshian et al., 2011; Zeng et al., 2018).

* Corresponding author.
E-mail addresses: jsolakia@gmu.edu (J. Solakian), vmaggion@gmu.edu (V. Maggioni), adlodhi@vt.edu (A. Lodhi), agodrej@vt.edu (A. Godrej).

https://doi.org/10.1016/j.ejrh.2019.100630
Received 17 June 2019; Received in revised form 6 September 2019; Accepted 19 September 2019
Available online 01 October 2019

Due to the lack of ground-based monitoring systems and rain gauge networks, large scale hydrologic models often rely on remotely-sensed precipitation data from satellite sensors (Maggioni and Massari, 2018). Precipitation, whether from rain gauges or satellites, is characterized by spatial and temporal variability as well as measurement errors. Although ground-based instrument networks, including rain gauges and radars, represent the most direct surface rainfall measurements and often provide measurements with high temporal frequency, there are many limitations with these systems. Not only are gauges restricted by point-scale observations, but they are also subject to false readings due to wind effects and evaporation. In addition to measurement errors, spatial interpolation of point-based observations adds uncertainty to the resulting gridded precipitation datasets (Habib et al., 2012a; Li et al., 2008; Maggioni et al., 2016; McMillan et al., 2011). The spatial distribution and density of gauges play important roles in the adequacy of measurement. A number of studies found that hydrologic model uncertainty is greatly impacted by sparse and irregular rain gauge networks and that uncertainty is reduced by increasing gauge density, or by optimizing the distribution pattern (Bardossy and Das, 2008; Girons Lopez et al., 2015; Moulin et al., 2009; Maggioni et al., 2017; Zeng et al., 2018). Conversely, ground-based radar networks often provide continuous spatial coverage with high spatial and temporal resolution, but they are also limited in accuracy by attenuation and extinction of signal, surface backscatter, brightband effects, and uncertainty of the reflectivity-rain-rate relationship (Anagnostou et al., 2010; Habib et al., 2012a; Porcacchia et al., 2017). In addition to being limited in accuracy, both ground-based gauges and radars are often inadequate due to sparse availability, especially outside of the United States.

Satellite-based precipitation products (SPPs) offer a viable alternative to ground-based data through continuous monitoring of precipitation with greater spatial coverage. Over the past twenty years several studies have compared SPPs to in-situ ground observations, evaluating the use of SPPs as a resource in hydrologic modeling. Nijssen and Lettenmaier (2004) noted that major sources of satellite-based precipitation uncertainty arise from algorithmic miscalculations, as well as instrumentation and sampling errors. Hydrological modeling using SPPs as forcing input, particularly for simulations in large, complex watersheds involving heterogeneous land use (influencing soil moisture fluctuations and evaporation) and significant terrain changes, is not always adequate (Mei et al., 2014a, 2014b; Milewski et al., 2015; Seyyedi et al., 2015; Yang and Luo, 2014). For instance, SPPs often show an elevation-dependent bias with an underestimation of light precipitation at higher elevations (Maggioni et al., 2016). Mei et al. (2016); Villarini et al. (2011), and Xu et al. (2014) found that the accuracy of hydrologic model simulations from SPPs is impacted not only by product resolution but also by storm severity and basin scale, where the most accurate simulation of hydrologic models using SPPs is when a combination of moderate precipitation magnitudes, finer product spatial resolutions, and larger basin scales are associated with the model.

Aside from the 3 principal measurement sources used to determine precipitation (ground-based gauge observations, ground-based radars, and satellite remote sensing), precipitation estimates can be obtained from atmospheric retrospective-analysis models (Beck et al., 2017). Two of the most widely accepted atmospheric reanalysis datasets with long-term coverage are (i) the European Centre for Medium Range Weather Forecasts (ECMWF) ERA-Interim, a dataset that uses a 4-dimensional variational analysis, a revised humidity analysis, and variational bias correction for satellite data (Berrisford et al., 2011) and (ii) NASA's Modern Era Retrospective-analysis for Research and Applications (MERRA) (Rienecker et al., 2011). Moreover, there are products that combine a set of data from multiple methods (models and observations) and/or instruments (ground- and satellite-based). For instance, the Multi-Source Weighted-Ensemble Precipitation (MSWEP) is a fully global dataset from 1979 to 2017 at 3 -h and 0.1° temporal and spatial scales, respectively. This dataset uses various gauge, satellite, and reanalysis data to provide precipitation estimates globally (Beck et al., 2017). Though re-analysis datasets and blended products have the potential for providing good quality precipitation estimates (Beck et al., 2017; Duque-Gardeazábal et al., 2018; Ma et al., 2018), these products were not considered in this study since the use of blended products would not allow for the differentiation of results among instruments and algorithms.

A plethora of research has been conducted over the past 2 decades on the use of remote sensing products for hydrologic model simulation and predictions intended for flood forecasting, riverine modeling, and climate studies in complex terrains (Gebregiorgis and Hossain, 2013; Hussain et al., 2018; Mei et al., 2016; Sharifi et al., 2018) and across various climatic regions (Bitew et al., 2012; Guo and Liu, 2016; Guo et al., 2015; Milewski et al., 2015; Verdin et al., 2016). Where current research falls short is the application of SPP data in hydrologic models specifically aimed at simulating and forecasting water quality.

It is well understood that the intensity, frequency, and duration of precipitation have significant and direct impacts on runoff quantity and thus streamflow. In turn, precipitation is also a major driver of water quality. A number of studies evaluating and quantifying predictions of stream water quality has demonstrated that spatial-temporal variations of water quality is strongly dependent on the spatial and temporal scales of analysis (Barakat et al., 2016; Bengraïne and Marhaba, 2003; Chang, 2008; Jeznach et al., 2017; Kang et al., 2010; Mei et al., 2014a, 2014b; Wang et al., 2011; Wunderlin et al., 2001; Xu et al., 2012). The relationship between water quality indicators and streamflow has been investigated using both parametric (distribution-dependent) and non-parametric (distribution-free) methods (Azhar et al., 2015; Barakat et al., 2016; Bu et al., 2010; Chang, 2008; Fovet et al., 2018; Johnson et al., 2012; Jung et al., 2016; Kisi and Ay, 2014; Nóbrega et al., 2018; Noori et al., 2010; Soler et al., 2007; von Freyberg et al., 2017). All of these past studies demonstrated a direct impact in water quality as it relates to streamflow.

This study fills this gap in the literature, by evaluating the performance of a hydrologic model, forced with 3 SPPs, in estimating water quality indicators in the Occoquan Watershed, located in the northern Virginia suburbs of Washington D.C., United States. The overarching purpose of this study is to determine the suitability of SPPs as a substitute for rain gauge precipitation data for simulating selected water quality indicators. In this study, the satellite products are compared to the data collected by a dense rain gauge network to determine their capability of (1) accurately characterizing the spatial and temporal variability of precipitation within the study region, and (2) simulating water quantity and quality in the Occoquan Watershed. Section 2 describes the study area and the data sets adopted in this work; Section 3 introduces the methodology; Section 4 presents and discusses the results; and Section 5 highlights the main conclusions, limitations, and future directions.

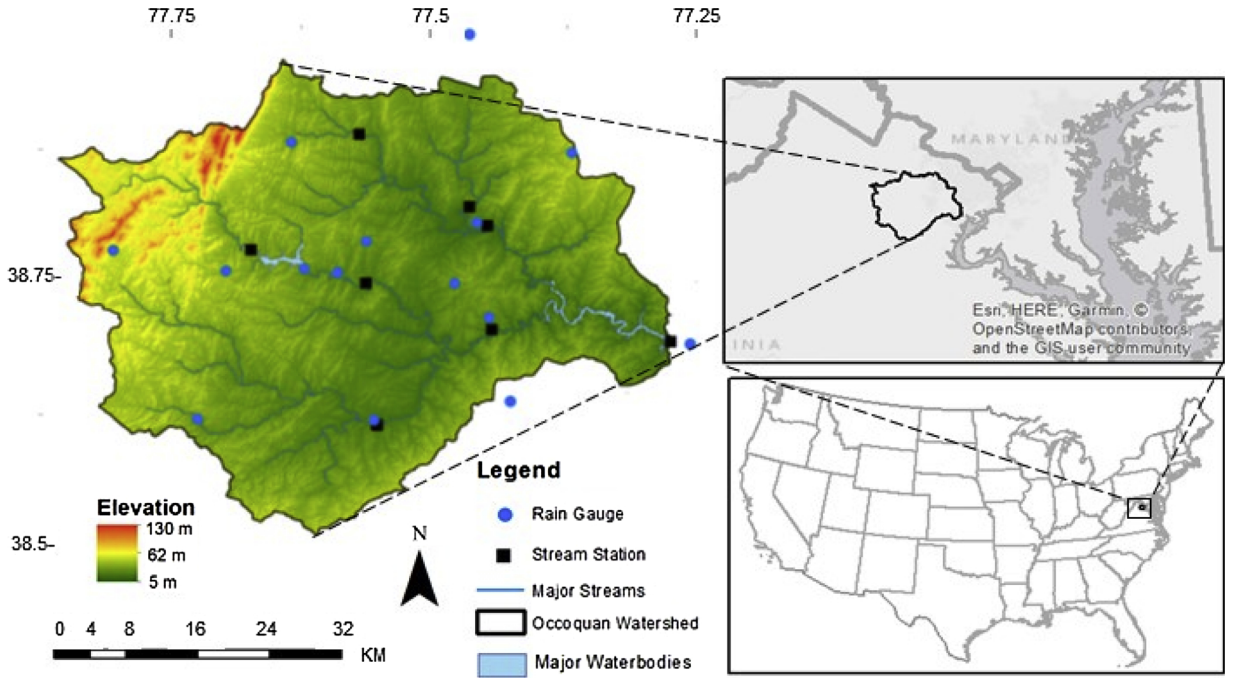

Fig. 1. Map of the study area showing the watershed boundary, topography, major streams, major waterbodies, and locations of stream monitoring stations and rain gauges.

2. Study area and data sets

2.1. Study area

The focus of this study is the Occoquan Watershed, a 1500 sq. km area located in suburban Washington, D.C., in the northern portion of Virginia (Fig. 1). The watershed supplies water to 2 drinking water reservoirs: Lake Manassas and the run-of-the-river Occoquan Reservoir, which are part of the drinking water supply to approximately 2 million residents. The area is urbanized with a mix of suburban and urban land use and has mild topographic variation. The Occoquan Watershed is part of the Potomac River Watershed, ultimately discharging into the Chesapeake Bay.

The Occoquan Watershed has been a major focus of regulatory oversight for the past 40 years due to the unprecedented growth of the D.C. metropolitan area which resulted in a substantial increase in reclaimed domestic wastewater discharged to receiving waters in the watershed, the closure of 11 marginally-functioning water reclamation facilities (WRFs), and the construction of a single state-of-the-art WRF that currently receives wastewater from Prince William and Fairfax counties and the cities of Manassas and Manassas Park, and discharges to 1 of the 2 tributaries (Bull Run) of the Occoquan Reservoir. Since 1973 the Virginia Tech Occoquan Watershed Monitoring Laboratory has monitored the watershed through data acquisition from a network of rain gauges, meteorological stations and stream monitoring stations. Precipitation, streamflow and several indicators of water quality have been measured continuously throughout the watershed using automated rain gauges and steam monitoring stations, shown in Fig. 1 as blue dots and black squares, respectively. Some of the rain gauges were available online in the 2000-01 period. During the course of this study period (2008–2012), data were available from all stations presented in Fig. 1.

The Occoquan Watershed Monitoring Laboratory has also been using the U.S. Environmental Protection Agency's (EPA) Hydrologic Simulation Program FORTRAN (HSPF) model to simulate the hydrology, nonpoint source runoff, and water quality of the watershed (described in detail in Section 3.1). The model delineates 87 segments within the 7 catchments of the Occoquan Watershed, as depicted in Fig. 2. The two reservoirs—Lake Manassas and Occoquan Reservoirs—are simulated using the U.S. Army Corps of Engineers' developed 2-dimensional hydrodynamic and water quality model CE-QUAL-W2, but are not included in this study as they contribute very little to the water budget, except for the rain that falls directly on the reservoir water surfaces. The study period of 2008–2012 was chosen because the latest Occoquan model addresses that period. Land use in the watershed is updated every 5 years, the point at which the model is updated. At the time of this study, the 2008–2012 model, based on the 2010 land use, consisted of the latest available data.

2.2. Precipitation data

Ground-based precipitation observations are obtained from a network of 15 tipping bucket rain gauges, independently operated by the Occoquan Watershed Monitoring Laboratory, located within or approximate to the Occoquan Watershed (Fig. 1). The quality-

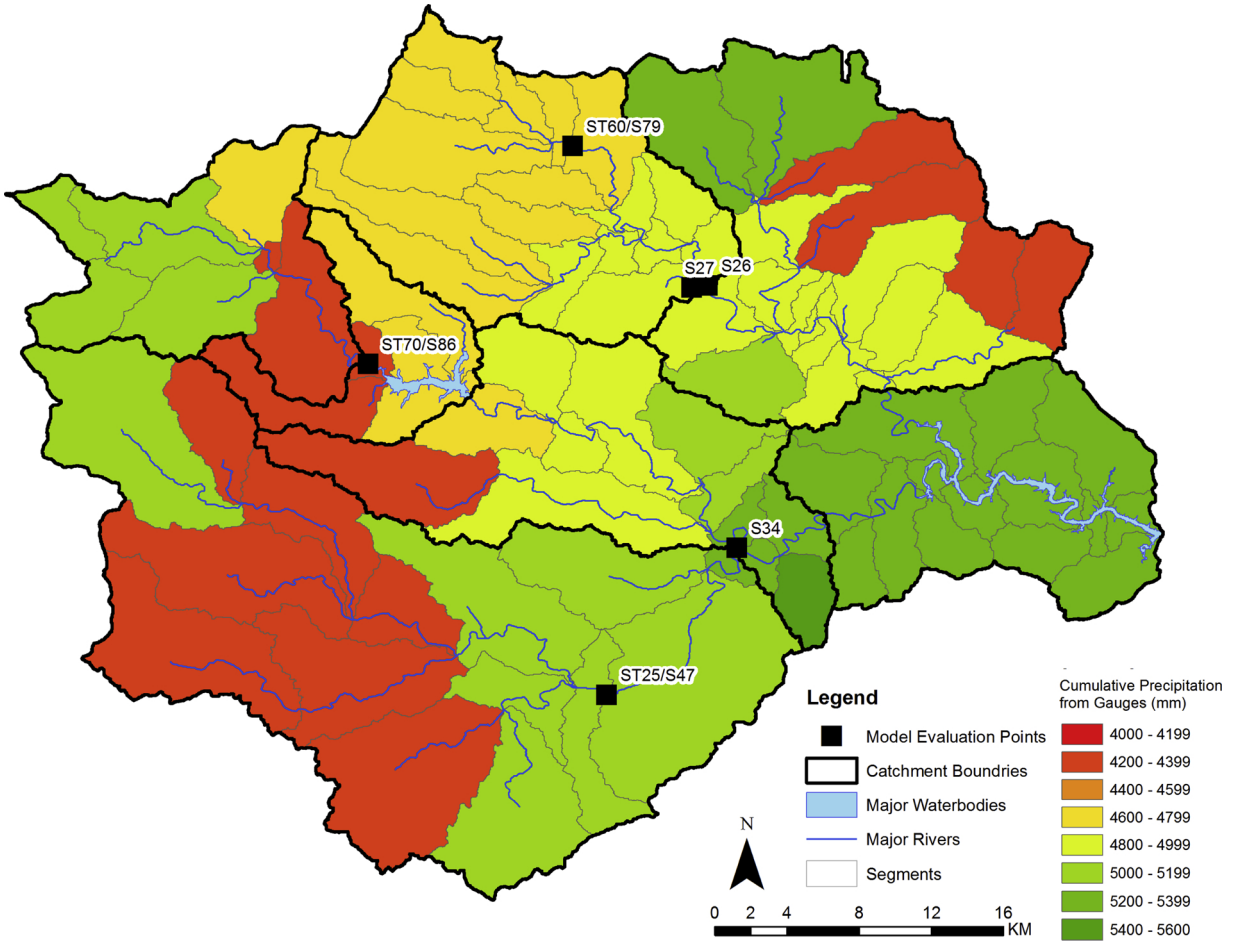

Fig. 2. Cumulative precipitation (mm) for each segment recorded by rain gauges during the 5-year study period including the delineation of 7 catchments and 87 segments, and the locations of study evaluation points.

controlled gauges collect precipitation measurements in increments of 0.254 mm (0.01 in.) by recording the time of occurrence of successive tips logged hourly throughout the 5-year temporal span of this study (2008–2012). While ground-based gauge observations are widely accepted as providing the most accurate method for precipitation measurement, tipping buckets have been known to experience significant levels of error at low rainfall intensities (Habib et al., 2012b) and may be sensitive to ground vibrations, wind effects, and orifice opening size. The density of gauges is also important when capturing variability of rainfall at fine temporal scales, for extreme events, or over complex terrain (Kidd et al., 2017). Additionally, many gauges are typically not able to measure snowfall accurately and therefore may underestimate the corresponding liquid precipitation equivalent (Rasmussen et al., 2012).

Alternatively, SPPs are used to estimate precipitation quasi-globally using a combination of remotely sensed microwave and infrared sensors. Here we adopt 3 of the most widely used SPPs: (1) the National Aeronautics and Space Administration (NASA) Tropical Rainfall Measuring Mission (TRMM) Multi-satellite Precipitation Analysis (TMPA) (Huffman et al., 2010); (2) the U.S. National Oceanic Atmospheric Administration (NOAA) Climate Prediction Center's (CPC) morphing technique (CMORPH) (Joyce et al., 2004); and (3) the Precipitation Estimation from Remotely Sensed Information using Artificial Neural Networks (PERSIANN)-Cloud Classification System (CCS) (Hsu et al., 2010). This study compares these 3 SPPs of varying spatial and temporal resolutions as forcing inputs of the hydrologic model to simulate water quality in the Occoquan Watershed. The main characteristics of precipitation products used in this study are summarized in Table 1.

The TRMM satellite mission was launched in 1997 and ceased in 2015. During that time TRMM-based products provided rainfall rates over the tropics and subtropics between 50 °N-50 °S (Huffman et al., 2007, 2010). Specifically, the TMPA algorithm combines both infrared and microwave sensor data to produce precipitation products with a spatial resolution of 0.25° and a temporal resolution of 3 h in both real-time and latent calibrated versions (3B42-RT and 3B42-V7, respectively). This study uses the bias-adjusted 3B42-V7 product, which will be herein referred to as TMPA.

The CMORPH algorithm produces global precipitation analyses at high-resolutions using precipitation estimates derived exclusively from low orbiter satellite microwave observations transported via spatial propagation information obtained from geostationary satellite data (Joyce et al., 2004). CMORPH interpolates precipitation features between consecutive microwave sensor

Table 1
Characteristics of precipitation products used in study, including the percentage of missing records during the study period (2008–2012).

	Spatial Resolution	Temporal Resolution	Domain Coverage	# Pixels/ Points Covering Study Area	Missing Records
TMPA 3B42V7	0.25°	3 hour	50 °N – 50 °S	6	0.01%
CMORPH	0.07°	30 min	60 °N – 60 °S	48	0.35%
PERSIANN-CCS	0.04°	30 min	60 °N – 60 °S	133	0.48%
Rain Gauge Network	Point-source	1 hour	Watershed	15 gauges	< 0.01%

samples aboard multiple spacecrafts. Product data cover the 60 °N-60 °S area over a period of record from December 2002 to present-day. Data used in this study are reprocessed and the bias corrected at a spatial resolution of ~8 km (exactly 8 km at equator/0.07°) and a 30-minute temporal frequency. Bias correction is performed by matching CMORPH raw data against the CPC daily gauge analysis over land (Xie et al., 2017).

PERSIANN − CCS, first released in 2003, is an algorithm based on infrared brightness temperature that extracts cloud features from a number of geostationary satellites operated by several agencies covering an area between 60 °N and 60 °S (Hong et al., 2007; Hsu et al., 1997; Sorooshian et al., 2000). Precipitation estimates are assigned using infrared cloud images from segmented cloud features such as statistics, textures, and geometry at brightness temperature thresholds. This information is used to obtain a relationship between brightness temperature and rainfall rates. The PERSIANN − CCS algorithm uses gauge-corrected radar hourly rainfall data to calibrate cloud-top brightness temperature and rainfall relationships for the classified cloud groups in order to estimate precipitation (Hong et al., 2007). PERSIANN − CCS (hereafter called PERSIANN) is available at a spatial resolution of 0.04° and a 30-minute temporal frequency.

Gauge observations are interpolated to each of the 87 segments in the watershed using the nearest-neighbor method. Cumulative precipitation of the interpolated gauge data during the study period is shown in Fig. 2 for each segment of the Occoquan Watershed. Fourteen (14) of the 15 rain gauges across the study area provide hourly records; however, 1 gauge (LRTN 150), located at the downstream extents of the watershed, collects records at a daily scale. The observations from this gauge are used as precipitation input to 6 segments (S54, S60-S63, and S78) located in the Occoquan catchment. Daily records collected at LRTN 150 are disaggregated to hourly values for input into the HSPF model. The percentage of missing records provided in Table 1 does not include missing hourly records for gauge LRTN 150.

The SPPs are processed by spatially averaging all pixels falling within the boundaries of each watershed segment. Since each satellite precipitation product is provided in a different temporal resolution, all satellite data matched to the hourly temporal scale. The spatially interpolated gauge data and spatially averaged satellite products at the hourly scale are used as input to the HSPF model to simulate streamflow and water quality indicators (discussed in Section 3.3). Since the Occoquan HSPF model output is set to output at a daily scale, precipitation data is subsequently aggregated to daily values for comparison of the SPPs (input data and output results) to the gauge-based data (Section 3.2).

2.3. Stream monitoring stations

Streamflow, stream stage, and water quality are measured at 8 stations across the watershed. Flow and stream stage are continuously measured by automated equipment including a Sutron datalogger and flow meter. Flow and stage are continuously measured and recorded on an hourly basis provided there is no change. When there is a change in flow, such as during storm events, flow and stage are recorded every 15 min until streamflow and stage are normalized (Xu et al., 2007). Water quality samples for baseflow conditions are typically obtained once each week, and storm samples are composited in the field using an automated sampler paced to sample equal aliquots for equal volume of flow that passes the sampling point, then adding these to a compositing bottle. Water quality parameters including stream temperature (TW), concentrations of total suspended solids (TSS), orthophosphate phosphorus (OP), ammonium nitrogen (NH_4-N), nitrate-nitrogen (NO_3-N), dissolved oxygen (DO), biochemical oxygen demand (BOD), and total organic carbon (TOC) are obtained for all samples. Observed information at the 8 stations is used to calibrate and validate the hydrologic and water quality model analyzing the Occoquan Watershed. While data from 8 stations are used for model calibration and validation, this study analyzes results from 3 monitoring stations (ST25, ST60, and ST70) specifically for streamflow, TW, TSS, DO, and BOD, which is discussed in detail in Section 3 and 4.

3. Methodology

The first step in this study is to compare each SPP (TMPA, CMORPH, and PERSIANN) to the dense rain gauge network in the Occoquan Watershed in order to identify differences among the satellite products in the region. Then, the hydrologic model is forced with each satellite product and the traditional rain gauge dataset at the hourly scale to simulate streamflow and water quality indicators in the watershed during the 5-year study period (2008–2012). Model outputs are evaluated by comparing the results of daily simulated streamflow and selected water quality indicators from the 3 SPP simulations to that of the reference model simulation forced with rain gauge-based records.

3.1. Hydrological model

The HSPF conceptional lumped hydrological model, developed by the Occoquan Watershed Monitoring Laboratory, is designed to simulate various hydrological processes and associated water quality components in the Occoquan Watershed (Xu et al., 2007). The model is updated every 5 years with current land use information classified into 14 land use categories based on impervious coverage and soil properties obtained from the Northern Virginia Regional Commission and is modeled in 5-year increments with in-situ meteorological data: air temperature, cloud cover, dew point temperature, wind speed, solar radiation, potential evapotranspiration, and precipitation. Air temperature, cloud cover, dew point temperature, wind speed, and solar radiation are all directly measured at the National Oceanic and Atmospheric Administration (NOAA) weather station located at the Washington Dulles International Airport (Dulles station) approximately 27 km from the centroid of the Occoquan Watershed. Hourly readings of the aforementioned data from this station are applied to the model each hour as 1 uniform input to the entire watershed for those parameters. Since a direct measurement of potential evapotranspiration is not available from the Dulles meteorological station used in this study, potential evapotranspiration was calculated from the modified Penman Pan empirical method using air temperature, dew point temperature, wind movement, and solar radiation obtained from the Dulles station. The temporal and spatial resolution of the retrieved land use data and all meteorological data (i.e., air temperature, cloud cover, dew point temperature, wind speed, solar radiation, and potential evapotranspiration), aside from precipitation, are consistently maintained and are not altered in any way during model simulations. Precipitation input is retrieved on an hourly basis from the 15 rain gauges within or in proximity to the watershed boundaries. Although neither an evaluation of the parameter input, including land use and meteorological data, nor a validation of the long-established HSPF hydrology model, is within the scope of this study, a brief description of the model's setup is described herein. For additional details of model setup and execution, we refer the reader to Xu (2005, 2007) and Maldonado and Moglen (2012).

Precipitation input is retrieved and inputted for each segment from the nearest-neighbor rain gauge, while all other meteorological data used in the model (air temperature, cloud cover, dew point temperature, solar radiation, wind speed, and wind direction) are applied consistently throughout all 87 segments. During certain periods of this 5-year study, rain gauge observations are not recorded at various gauges. Missing precipitation records are interpolated since the HSPF model requires continuous precipitation input. For missing gauge records, a standardized procedure is employed to estimate the discrete hourly values based on the spatial and temporal infilling strategy outlined by Xu (2005). A similar infilling strategy is applied to missing precipitation data for TMPA, CMORPH, and PERSIANN during the study period. Using similar procedures outlined in multiple meteorological infilling studies (Hema and Kant, 2017; Kim and Ryu, 2015; Lee and Kang, 2015) and recommended by the U.S. EPA (2000), meteorological data gaps are classified into categories based on gap duration. For gaps up to 4 h, temporal linear interpolation is applied. For gaps greater than 4 h, a combination of temporal linear interpolation and nearest-neighbor pixel value is utilized. Precipitation input from each satellite product is then aggregated for each segment.

The watershed is comprised of 87 segments within distinct 7 catchments (Table 2, Fig. 2). Each of the 7 catchments has a separate HSPF model that is linked to create the overall watershed model. The HSPF model used in this analysis is deterministically calibrated and validated between simulated gauge-based results and observed data over a 5-year period from January 1, 2008 to December 31, 2012. While HSPF is able to produce output results as low as 15-minute increments (which is the increment flow data are recorded and used for model input), the Occoquan HSPF model is set to output results using a daily scale. The daily scale is used to minimize the impacts of timing errors often found using lower increment outputs since HSPF is prone to timing errors, such as under- or over-predicting when an event starts and/or stops. Each catchment HSPF model is calibrated and validated prior to linking into the adjoining downstream model. Eight (8) stream monitoring stations throughout the watershed that collect streamflow, stream stage, and water quality constituents are used to calibrate the HSPF model. The model is first calibrated on both daily and monthly streamflow by comparing simulated flows from gauge records with observed data from stream monitoring stations during the first 2 years of the study period (2008–2009). Results of the simulated model are then validated for an independent period (2010–2012). The model provides output for streamflow and water quality indicators including TW, TSS, OP, TP, NH_4-N, NO_3-N, TN, DO, BOD, and TOC. Next, the model is calibrated for TSS, TW, OP, NH_4-N, and NO_3-N based on monthly and yearly loads to that of observed in-stream data.

The HSPF model is used to simulate streamflow and select water quality indicators at 6 designated evaluation points in the Occoquan Watershed. These 6 locations are located within 3 distinct catchments (Cedar Run, Upper Broad Run, and Upper Bull Run), which capture runoff from a number of segments of varying size, land use, and topography (Table 2, Fig. 2). Of the 6 model evaluation points, 3 points (S47/ST25, S79/ST60, and S86/ST70) are equipped with stream monitoring stations, which are also used

Table 2
Drainage areas associated with model simulated evaluation points.

Evaluation Point	Catchment	Drainage Area (km^2)
S27	Segment 27 of Upper Bull Run	17.81
S79/ST60	Upper Portion of Upper Bull Run	63.63
S86/ST70	Upper Broad Run	126.44
S26	Upper Bull Run (excl. Seg 27)	186.24
S47/ST25	Upper Portion of Cedar Run	394.26
S34	Cedar Run	498.42

Table 3
Error statistics of calibrated individual catchment-based HSPF models at 3 model evaluation points (S47/ST25, S86/ST70 and S79/ST60) for streamflow and select water quality indicators (TW, TSS, and DO).

	S47/ST25			S79/ST60			S86/ST70		
	NSE	RMSE	rB (%)	NSE	RMSE	rB (%)	NSE	RMSE	rB (%)
Daily streamflow (m^3/s)	0.70	0.55	−5.19	0.79	0.46	−6.14	0.77	0.48	−0.88
Monthly streamflow (m^3/s)	0.79	0.46	−4.94	0.84	0.40	−6.14	0.80	0.44	−3.31
Daily TW (°C)	0.92	0.28	−0.37	0.85	0.39	−0.73	–	–	–
Daily DO (mg/l)	−1.35	1.53	11.96	0.56	0.66	−2.03	0.61	0.63	2.26
Monthly TSS (mg/l)	0.62	0.61	10.81	0.74	0.51	−2.17	0.75	0.50	−5.85

in the original model calibration/validation process. The streamflow error analysis performed with respect to in-stream observations reveal a well calibrated model at each of the 3 observation locations (S47/ST25, S79/ST60, and S86/ST70). Error analyses of TW and DO at a daily scale and TSS at a monthly scale also show good model skills at the 3 locations (Table 3) in terms of Nash-Sutcliffe Efficiency (NSE), relative bias (rB), and root-mean-square error (RMSE) (Eqs. (1)–(3)). Optimal values of NSE, rB, and MSE are 1, 0, and 0, respectively.

$$NSE = 1 - \left[\frac{\sum_{i=1}^{n} (Q_{si} - Q_{oi})^2}{\sum_{i=1}^{n} (Q_{oi} - \bar{Q}_s)^2} \right] \quad (1)$$

$$rB = \left[\frac{\sum_{i=1}^{n} (Q_{si} - Q_{oi})}{\sum_{i=1}^{n} (Q_{oi})} \right] \text{x } 100\% \quad (2)$$

$$RMSE = \sqrt{\frac{\sum_{i=1}^{n} (Q_{si} - Q_{oi})2}{n}} \quad (3)$$

Where n is the total number of events, Q_{oi} is the *i*th observed streamflow or water quality indicator value, Q_{si} is the *i*th simulated satellite-based streamflow or water quality indicator value, $\bar{Q}$ is the corresponding mean value and n is the number of values. NSE is dimensionless whereas RMSE is provided in respective units (m^3/s, °C, mg/l) and rB is a percentage.

The model is next forced with precipitation data from each of the 3 SPPs to simulate streamflow and water quality at the 6 evaluation points.

3.2. Precipitation analysis

As previously discussed, hourly precipitation data were areal-weighted and segment-aggregated (AWSA) for input into the model. The hourly data were then aggregated to the daily scale for comparison with the ground observations. Precipitation was evaluated at the daily scale for consistency with the daily model output results. Several metrics are considered to quantify the performance of SPPSs: RMSE, Pearson correlation coefficient (PCC), Standard deviation (σ), and bias (B). The RMSE, a measure of the differences between SPP and observed (gauge) values, combines the magnitude of errors in the estimation over time into a single measure of error. The PCC is the average product of the deviation of variables from their respective means, divided by the standard deviation of those variables. Standard deviation is used to quantify the amount of variation in the data set. B measures the average tendency of satellite data to either overestimate or underestimate the gauge measurements, whereas rB evaluates the relative difference in percentage between the estimated and the observed data. Optimum values of PCC, σ, and B are 1, 0, and 0, respectively. The definitions of the statistical metrics are provided in Eqs. (3)–(6).

$$PCC = \frac{\sum_{i=1}^{n} (P_{oi} - \bar{P}_o)(P_{si} - \bar{P}_s)}{\sqrt{\sum_{i=1}^{n} (P_{oi} - \bar{P}_o)^2} \sqrt{\sum_{i=1}^{n} (P_{si} - \bar{P}_s)^2}} \quad (4)$$

$$\sigma = \sqrt{\frac{1}{n} \sum_{i=1}^{n} (P_i - \bar{P})} \quad (5)$$

$$B = \frac{\sum_{i=1}^{n} (P_{si} - P_{oi})}{n} \quad (6)$$

Where n is the total number of events, P_{oi} is the *i*th observed rain gauge precipitation or observed streamflow and P_{si} is the *i*th simulated satellite precipitation or simulated streamflow, $\bar{P}$ is the corresponding mean value. PCC is dimensionless whereas σ and B are in mm/d. The RMSE, PCC, and σ are summarized using a Taylor diagram (Taylor, 2001), which shows the overall skill associated with each SPP in relation to the gauge-based dataset (Section 4.1).

Probability of detection (POD), false alarm rate (FAR), and critical success index (CSI) are used to assess the detection capability of each SPP based on the AWSA daily precipitation. POD corresponds to the ratio of correct detection of the SPP to the overall

occurrence of precipitation observed. Conversely, FAR indicates the number of cases when precipitation is estimated by SPP; however, no precipitation is observed. CSI is a measure of events successfully detected by the SPP to the total number of events observed that are either made or needed (Schaefer, 1990). These metrics all range from 0 to 1, with the accuracy of the SPP increasing as the FAR approaches 0 and the POD and CSI approach 1. Optimum values of POD, FAR, and CSI are 1, 0, and 1, respectively. For this study, the precipitation threshold is set to 0.254 mm/day, which is the threshold of the rain gauges. POD, FAR, and CSI are calculated using Eqs. (7)–(9), where hits, misses and false alarms represent the total number of SPP observations that either correctly detect an event, miss, an event, or incorrectly detect an event, respectively, in relation to the gauge observation.

$$POD = \frac{Hits}{Hits + Misses} \tag{7}$$

$$FAR = \frac{False\ alarms}{Hits + False\ alarms} \tag{8}$$

$$CSI = \frac{Hits}{Hits + False\ alarms + Misses} \tag{9}$$

Detection metrics are summarized using a performance diagram (Roebber, 2009) that presents the POD, success ratio (1-FAR), CSI and B associated with each SPP in relation to gauge-based data for the 5-year study period (Section 4.1).

3.3. Streamflow and water quality analysis

It is well understood that there is a direct relationship between precipitation and streamflow. Research has also shown a significant and quantifiable correlation between atmospheric conditions and water quality indicator response (Chang et al., 2015; Gelca et al., 2016; Jeznach et al., 2017; Johnson et al., 2012; Murdoch et al., 2000; Soler et al., 2007; Thorne and Fenner, 2011). Water quality analysis for this study focuses on TW, TSS, DO and BOD. By definition TSS are particles that are larger than 2 µm whereas anything smaller than 2 µm is typically considered a dissolved solid. Since TSS is a specific measurement of all suspended solids, organic and inorganic, by mass, it is a good representation of the total sedimentation rate of a watershed. TSS is both a visible and quantifiable indicator of overall water quality in a waterbody and therefore is selected for further evaluation in this study. DO is the measurement of gaseous oxygen dissolved in an aqueous solution which results from diffusion, by aeration, and as a product of photosynthesis. DO is an important indicator, determining the health and quality of a waterbody for its ability to support life. Similarly, BOD is the amount of DO needed by aerobic organisms to break down organic matter.

Three (3) statistical metrics (PCC, RMSE, and B) are used to evaluate the performance of the model in simulating streamflow and the 4 water quality indicators. The model simulation forced with rain gauge observations is used as a benchmark to assess the performance of the simulations forced with the 3 different SPPs. Uncertainties are quantified for simulated streamflow and selected water quality indicators at 6 evaluation points (S26, S27, S34, S47/ST25, S79/ST60, and S86/ST70) of varying drainage area within the watershed, discussed in detail in Section 4.2.

4. Results and discussion

4.1. Evaluation of satellite-based precipitation products

Fig. 3 presents the spatial distribution of cumulative precipitation over the 5-year study period for each SPP at their original pixel resolutions (left panels) and their corresponding areal-weighted value for each segment in the watershed. Foremost, Fig. 3 highlights the degree of detail for which each precipitation product is available (i.e., a total of 6, 48, and 133 precipitation values for TMPA, CMORPH and PERSIANN, respectively). In terms of cumulative precipitation within the watershed during the 5-year study period, the gauges recorded 4909 mm on average, whereas TMPA, CMORPH, and PERSIANN resulted in 5298 mm, 5267 mm, and 5834 mm, respectively, therefore PERSIANN showing the largest overestimation with respect to the reference dataset. TMPA shows the overall lowest variability of precipitation values, which can be attributed to its coarse spatial resolution and consequent low representativeness of the local precipitation distribution (only 6 pixels covering the entire watershed).

The SPPs are compared to gauge observations for all 87 segments of the watershed. This comparison is based on the interpolated and aggregated AWSAs rather than a pixel-to-point comparison, since the main focus of this study is to assess the impact of using different precipitation forcing datasets on simulating streamflow and water quality indicators in the watershed. AWSA satellite precipitation records aggregated to daily values are compared to daily aggregated gauge-based records. RMSE, PCC, and σ are calculated and plotted in a Taylor diagram to assess the performance of each SPP with respect to the gauged-based data (Fig. 4a). For the 3 products, correlation coefficients are concentrated between 0.26 and 0.60 and RMSEs range from 7.25 to 9.17 mm/day. The standard deviations of both TMPA and CMORPH are 8.08 mm/day, which is most likely due to the fact that these products use very similar input retrieval data in their algorithms. The standard deviation of PERSIANN, however, is lower (6.90 mm/day), which may be due to the fact that PERSIANN only uses one source (infrared) of observation data, whereas TMPA and CMORPH use both passive microwave and infrared observations. The best overall performance is from the CMORPH product, followed closely by TMPA. PERSIANN shows overall relatively inferior performance with low correlation values against gauge-based records. While both TMPA and CMORPH show good agreement with gauge-based records, both products overestimate precipitation magnitude (rB = 20.6% and 13.0%, respectively).

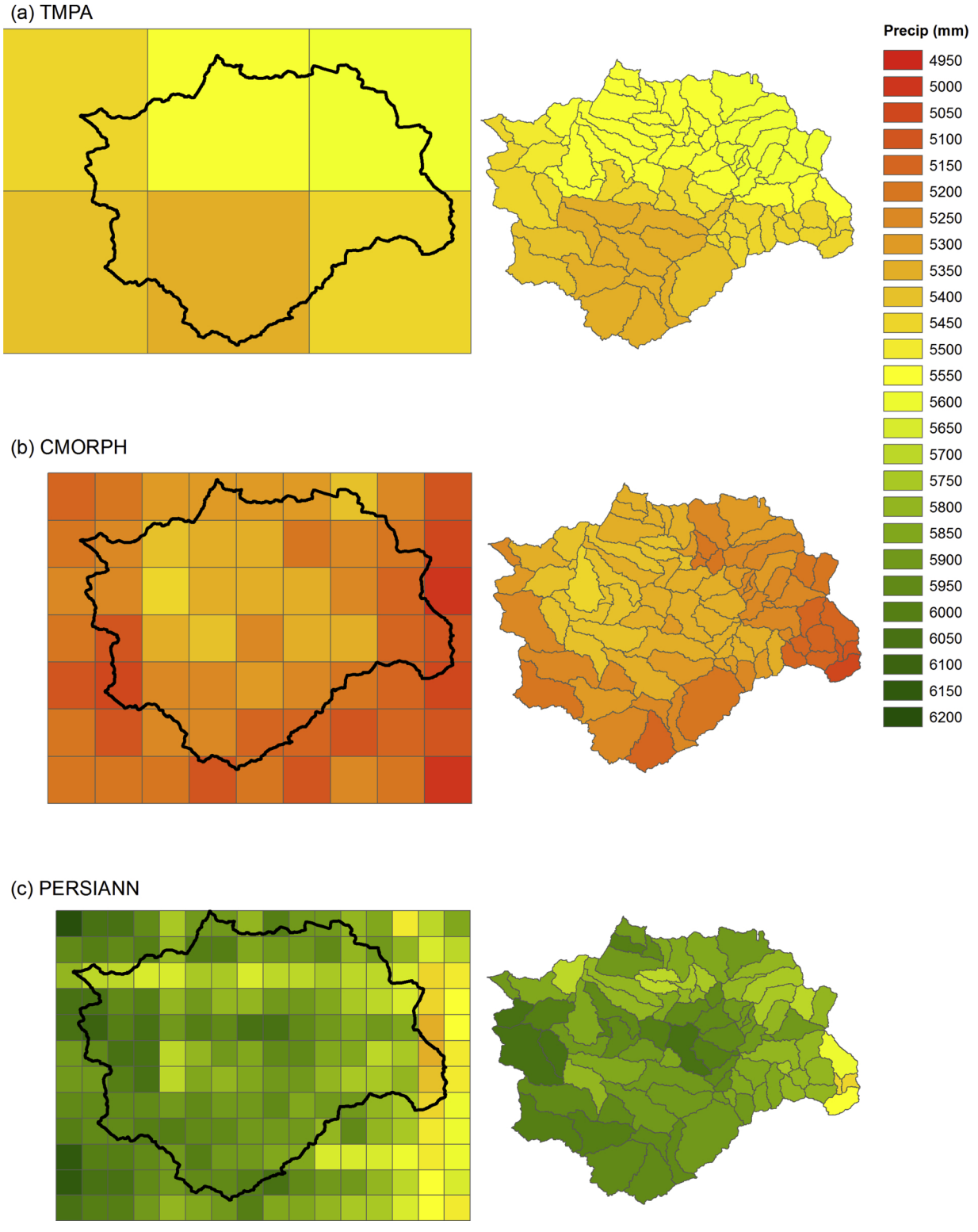

Fig. 3. 5-year cumulative precipitation over the satellite grid (left panels) and aggregated for each segment in the Occoquan Watershed (right panels) for (a) TMPA, (b) CMORPH, and (c) PERSIANN.

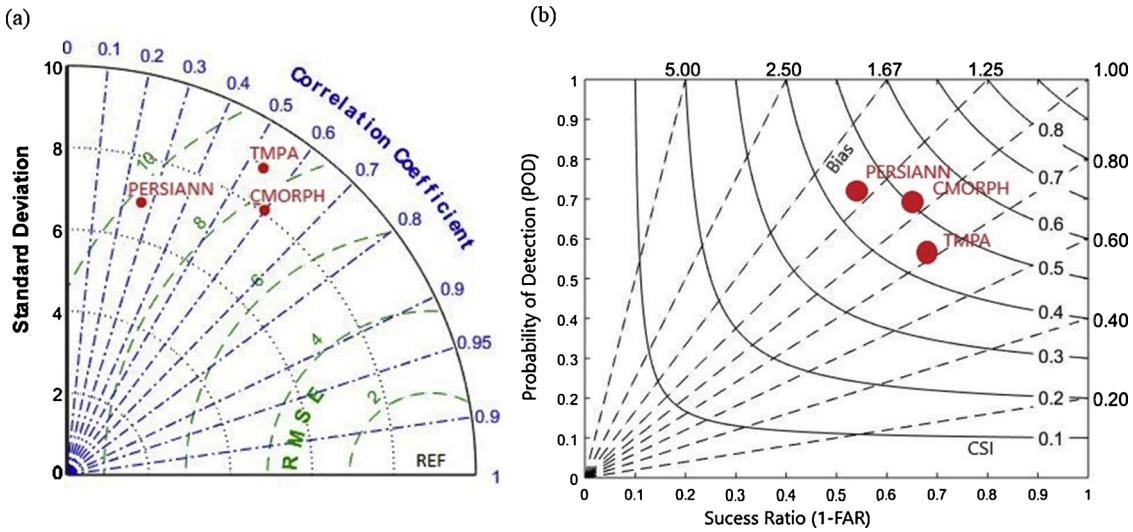

Fig. 4. (a) Taylor diagram and (b) Performance diagram of segment-aggregated daily precipitation between gauge-based observation and SPPs during 2008–2012.

The Performance diagram (Fig. 4b) suggests that both TMPA and CMORPH have lower false alarm rates (0.30 and 0.33, respectively) compared to PERSIANN, which exhibits a false alarm rate of 0.46. However, PERSIANN presents a higher probability of detection at 0.71 compared to TMPA (0.57) and CMORPH (0.68), respectively. B is relatively low for both TMPA and CMORPH at 0.51 and 0.39 mm/d, respectively, while PERSIANN has a slightly higher bias of 0.70 mm/d. TMPA and CMORPH exhibit similar performances, whereas simulation results derived from PERSIANN are quite different and show larger error metrics. This is most likely due to the fact that CMORPH and TMPA merge observations from passive microwave and infrared sensors, whereas PERSIANN only uses infrared observations.

Our results corroborate what was previously observed in the scientific literature. As summarized by Maggioni et al. (2016), mean errors and detection capabilities of satellite precipitation estimation vary across precipitation products and different regions of the world. A positive bias and season-dependent magnitude are reported over the contiguous United States for both CMORPH and PERSIANN-CSS. TMPA 3B42 is reported as having the lowest bias when compared to other satellite datasets. Furthermore, TMPA 3B42 exhibits a low probability of detection and low false alarm rate, whereas CMORPH has a higher probability of detection and also a larger number of false alarms. PERSIANN has both the highest false alarm rate and highest probability of detection compared to other products (Ebert et al., 2007; Yang and Luo, 2014). Results of this study validate that PERSIANN has the highest false alarm rate and probability of detection compared to TMPA and CMORPH within this study region.

4.2. Evaluation of simulated streamflow and water quality indicators

This section assesses the skills (PCC, RMSE, and B) of the complex-linked HSPF model of the Occoquan Watershed in terms of both streamflow and water quality indicators (TW, TSS, DO, and BOD). Specifically, we evaluate the simulations forced with the 3 different SPPs (TMPA, CMORPH, and PERSIANN) with respect to the reference run forced with gauge-based precipitation data. Aside from altering precipitation input, no other inputs, parameters, or model boundary conditions are modified in this experiment. Each of the 7 catchments that comprise the watershed are fairly uniform in topography, soil characteristics, and land use conditions; therefore, it is expected that these conditions will not have a significant impact to the uncertainty analysis based on drainage area size between SPPs and gauge-based simulations. The goal of this analysis is to quantify uncertainties in simulated streamflow and selected water quality variables at the 6 evaluation points (S26, S27, S34, S47/ST25, S79/ST60, and S86/ST70) in the watershed. These locations are chosen based on the representative basin scale ranging between 17.8 km^2 and 498.8 km^2 (refer to Table 2).

Fig. 5 shows that, for streamflow, CMORPH outperforms TMPA and PERSIANN in terms of all skill metrics. When compared to the gauge-forced simulation, CMORPH presents the highest correlation at all evaluation points with PCCs ranging from 0.47 to 0.75, nominally increasing as area increases, with a few exceptions. These exceptions are most likely due to differences in the hourly precipitation records of CMORPH, as well as TMPA and PERSIANN, in comparison to the rain gauge records in the Upper Broad Run catchment draining to S86/ST70. B and RMSE associated with streamflow also increase as area increases, with CMORPH marginally outperforming TMPA. PERSIANN shows the worst overall skill consistently for all basin scales. All 3 products overestimate daily streamflow in comparison to gauge-simulated streamflow, which is also observed in the precipitation analysis presented in Section 4.1. The increase of B and RMSE based on basin scale is expected since the streamflow, both simulated and observed at these points, increases and generates the potential for greater residuals.

In HSPF, most water quality variables are highly dependent on precipitation and its associated sediment and water flows, i.e., sediment loading and overland runoff flow (Duda et al., 2012). Satellite-based simulations of TSS showed the lowest skill among the

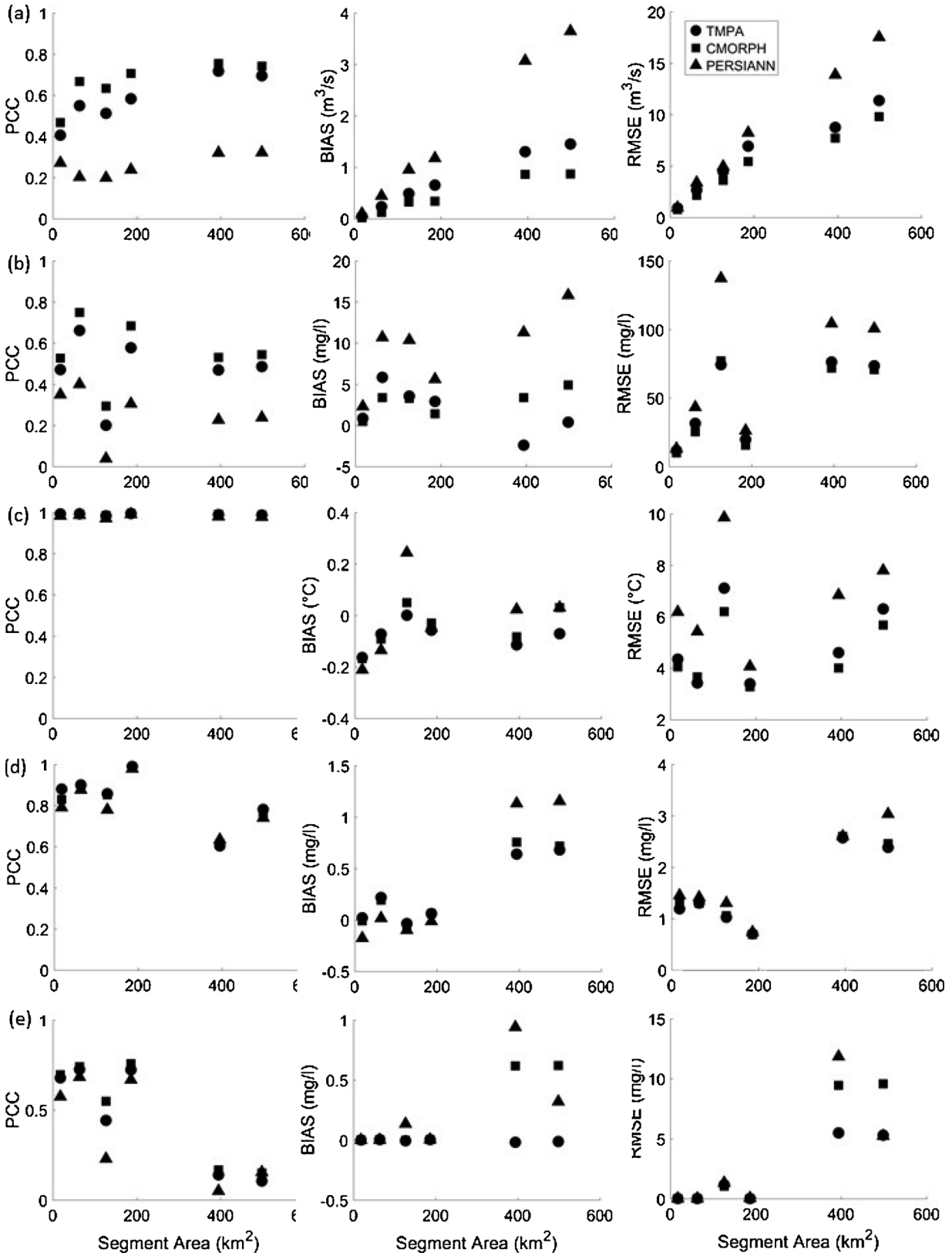

Fig. 5. Error plots by segment drainage area for daily records of (a) streamflow, (b) TSS (c) TW, (d) DO, and (e) BOD between gauge-based records and SPPs during the 2008–2012 study period.

water quality indicators evaluated in this study. Again, CMORPH showed the best performance among the SPPs, outperforming both TMPA and PERSIANN. PCC ranged from 0.20 to 0.66, 0.29 to 0.75, and 0.04 to 0.40 for TMPA, CMORPH, and PERSIANN, respectively. The lowest PCCs for all 3 products are at point S86/ST70, which also corresponds to the lower skill detected in the simulated streamflow. Each SPP overestimates TSS, with the exception of TMPA at point S47/ST25, though both TMPA and CMORPH, with a B of -2.4 to 5.8 m^3/s, and 0.46 to 4.9 m^3/s, respectively, have a considerably lower B than PERSIANN, which ranges between 2.3 and 15.8 m^3/s. For TSS, the basin extent seems to play a factor, showing generally decreasing PCC and increasing B and RMSE trends, as the drainage area increases. HSPF predicts sediment loading rates based on channel processes of deposition, scour, and transport that in turn determine both the total sediment load and outflow sediment concentrations in streamflow (Duda et al., 2012). Land use and soil type in the model are the major drivers for sediment load, calculated as total sediment for simulation of in-stream processes. Since land use is constant between the gauge-based and satellite-based simulations, there is no uncertainty or error associated with that input parameter. Therefore, precipitation, and consequently streamflow, is the major driver for TSS concentration differences presented in this analysis.

Simulated in-stream water temperature (TW) is well captured by all 3 SPP simulations with high correlations, ranging from 0.97 to 1.0, low biases, ranging from -0.21 to 0.24 °C, and low RMSEs, ranging from 3.3 to 9.9 °C. While stream temperature is impacted by precipitation, and thus streamflow, it is most closely correlated to ambient air temperature and therefore shows the lowest variation and highest skills among all output variables evaluated in this study. Generally, all 3 SPPs slightly underestimate TW, with a B of -0.16 to -0.06 °C for TMPA, 0.17 to 0.05 °C for CMORPH, and -0.21 to 0.03 °C for PERSIANN. Among all 6 evaluation points, only S86/ST70 overestimates TW consistently among all 3 products (0.00, 0.05 and 0.24 °C, respectively for TMPA, CMORPH, and PERSIANN), though CMORPH also overestimates TW at S34 and PERSIANN at S47.

Both DO and BOD show a large spatial variability among the 3 catchments having separate but interlinked HSPF models. PCC for DO is relatively high, ranging from 0.86 to 0.99, 0.83 to 0.99, and 0.78 to 0.98 for TMPA, CMORPH, and PERSIANN, respectively, in the Upper Bull Run and Upper Broad Run catchments. However, a decreasing skill for TMPA (0.60 and 0.78), CMORPH (0.62 and 0.75), and PERSIANN (0.63 and 0.74) in the Cedar Run catchment at locations (S47/ST25 and S34) is detected. Both B and RMSE show similar results of increased error with increasing drainage area in the Cedar Run catchment. B for all 3 products ranged from 0.02 to 0.68 mg/l, -0.01 to 0.76 mg/l, and 0.02 to 1.16 mg/l, for TMPA, CMORPH, and PERSIANN, respectively, while RMSE ranges from 0.71 to 2.57 mg/l, 0.69 to 2.60 mg/l, and 0.73 to 3.03 mg/l, for TMPA, CMORPH, and PERSIANN, respectively. In comparison to streamflow and TSS, the variability in the DO metrics is notably smaller, indicating that precipitation has moderate impacts on DO compared to other water quality indicators evaluated in this analysis.

Similar to DO, BOD has a satisfactory PCC in the Upper Bull Run catchment, but low PCC in the Cedar Run and Upper Board Run catchments, especially when PERSIANN is used as input precipitation. The model performs well in terms of B and RMSE in the Upper Bull Run and Upper Board Run catchments, but has low skill in the Cedar Run catchment (S47/ST25 and S34), with the exception of TMPA, which outperforms both CMORPH and PERSIANN in this catchment.

4.3. Temporal analysis of simulated streamflow and water quality indicators

As shown in the previous section, the positive bias in the SPPs is propagated into simulated streamflow, but not in all the water quality indicators. Here we analyze the temporal variability and seasonality of these variables. Fig. 6 shows time series of daily precipitation, streamflow, and water quality indicators (TSS, TW, DO, and BOD) at evaluation point S27 (the smallest drainage area among all areas considered in this study) for 1 year (2011) of the 5-year study. CMORPH and TMPA are able to decently capture the timing of the streamflow peaks, but tend to underestimate some peaks. While peaks in streamflow generally coincide with precipitation, it is evident that precipitation during the summer months (June through August) does not directly translate into streamflow. This may be due to a seasonal distribution within the model associated with an increased infiltration component. In HSPF, precipitation runoff is divided into surface runoff and infiltration. Infiltration then comprises of interflow, upper zone soil moisture storage, and percolation to lower zone soil moisture and groundwater storage. Within the HSPF model, increasing infiltration will reduce immediate surface runoff (including interflow) and increase the groundwater component, which is observed in Fig. 6 during summer months. It is also evident from Fig. 6 that PERSIANN overestimates precipitation in January and February, which is then rendered into an overestimation of both low and peak streamflow during cool months. Another factor impacting the observed decrease in streamflow during summer months may be due to the fact that higher evapotranspiration rates are typically seen in warmer months from increased ambient air temperature, which is sufficient to overcome the impact of increased humidity since drier soil tends to have increased infiltration rates compared to moister soil.

There is a direct relationship between streamflow and TSS concentrations (mg/l), with peaks well represented in both TMPA and CMORPH simulations. As with streamflow, TSS tends to be low throughout summer months aside from a few instances where intense precipitation is captured and translated into stream peak flow. Because PERSIANN overestimates streamflow in winter months, it in turn overestimates TSS concentrations during these months, since TSS is a flow-dependent variable, highly interrelated with streamflow. In-stream temperature is naturally dependent on ambient air temperature conditions, showing higher values in summer months and lower values in winter months. Aside from a few instances, all 3 SPPs follow the same TW trends as the gauge-based simulation.

As expected, concentrations of DO follow an inverse pattern with respect to TW, lower during warmer seasons and higher during cooler seasons. Simulated DO concentrations for all SPPs are fairly consistent with gauge-based simulations. Similar to gauge-based simulations, a strong flux in concentrations of DO is seen in warmer months which overlaps with streamflow low-flow periods. Comparatively, as shown in Fig. 6, it appears that PERSIANN displays the greatest number of daily fluctuations of BOD in comparison

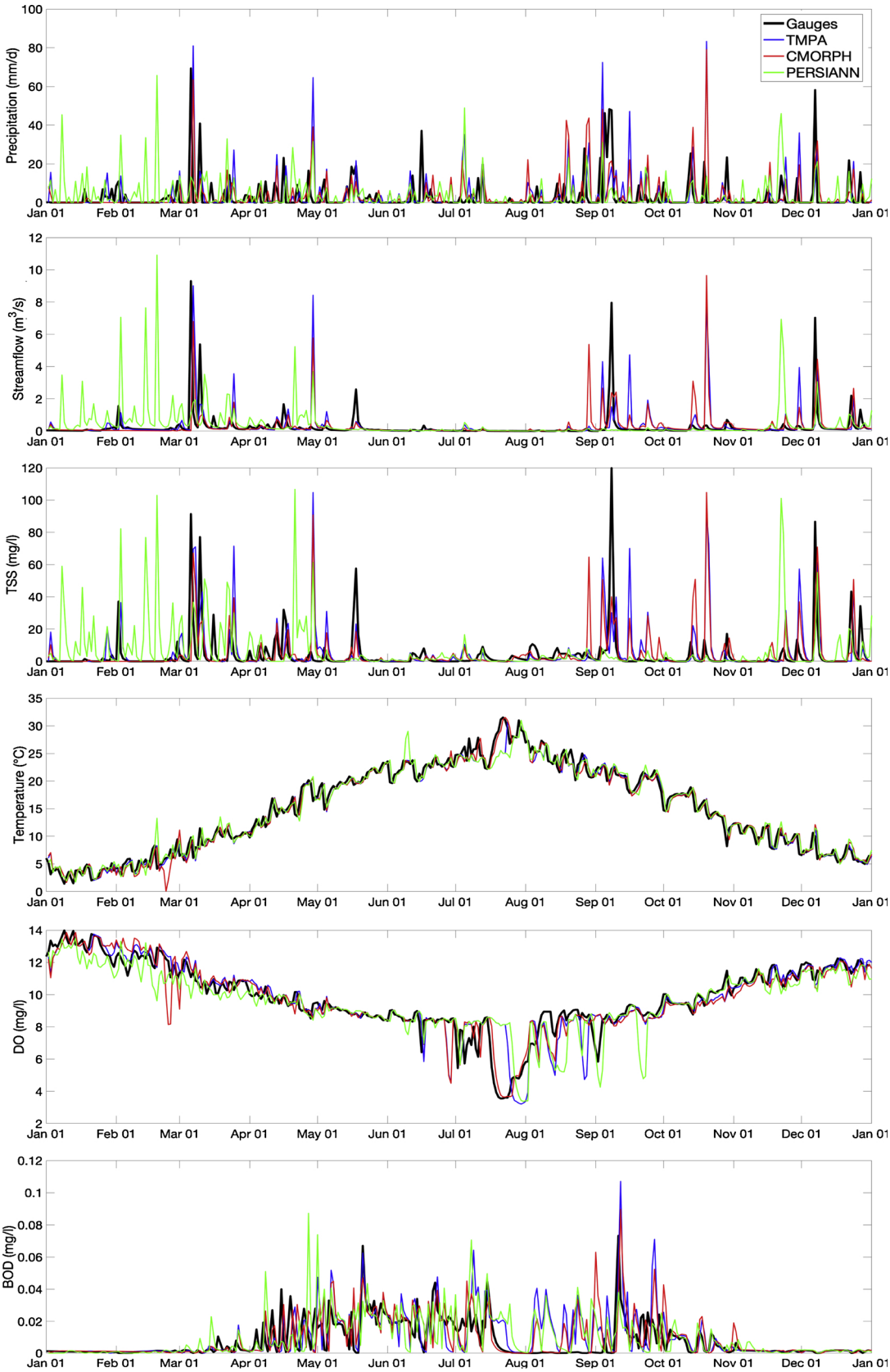

Fig. 6. Example daily time series for S27 during year 2011 of aggregated P (mm/d) and simulated streamflow (m^3/s), TW (°C), (TSS (mg/l), DO (mg/l) and BOD (mg/l) from gauge records, TMPA, CMORPH, and PERSIANN.

to TMPA and CMORPH. This fluctuation is especially true during January and February, which is likely due to the overestimation of precipitation during these months when compared to other products. Conversely, simulated BOD concentrations (mg/l) increase in warmer periods and drop during cooler periods following patterns associated with TW, yet this indicator also appears to be influenced by TSS concentrations during peak events.

5. Conclusions

This work investigated for the first time the potential of using SPPs for water quality monitoring and predictions. Three (3) SPPs (TMPA, CMORPH, and PERSIANN) of different spatial resolutions are compared to gauge-based records over a 5-year period (January 2008 – December 2012) across the Occoquan Watershed. This study provides a comprehensive analysis of the errors associated with streamflow and 4 water quality indicators (TW, TSS, DO, and BOD) simulated by forcing a hydrological model (the complexly-linked HSPF) with the 3 SPPs. These simulations are compared to a reference run, forced with gauge-based observations. The major findings of this research are summarized as follows:

- All 3 SPPs show moderate skill with respect to the daily gauge-based dataset. CMORPH shows the best overall performance, followed closely by TMPA. PERSIANN shows overall relatively inferior performance with low correlation with the gauge-based records. While both TMPA and CMORPH have good agreement with reference dataset, both products overestimate precipitation magnitude (rB = 20.6% and 13.0%, respectively). In terms of cumulative precipitation during the 5-year study period, PERSIANN shows the largest overestimation with respect to the gauges. TMPA shows the overall lowest variability, which can be attributed to its coarse spatial resolution and consequent low representativeness of the local precipitation distribution (only 6 pixels covering the entire watershed).
- Both TMPA and CMORPH present lower false alarm rates compared to PERSIANN across the Occoquan Watershed. However, PERSIANN presents a higher probability of detection compared to the other 2 products, especially during winter months.
- Satellite-based simulations of streamflow show that CMORPH outperforms both TMPA, and PERSIANN when compared to the reference simulation forced with gauge observations. CMORPH has the highest skill for daily streamflow across all evaluation points with a PCC ranging from 0.47 to 0.75, nominally increasing as drainage area increases. CMORPH and TMPA are able to capture the timing of the streamflow peaks well, but tend to underestimate some peaks. While peaks in streamflow generally coincide with precipitation, it is evident that precipitation during the summer months (June through August) do not directly translate to streamflow.
- Satellite-based simulations of TSS show the lowest skill among the water quality indicators evaluated in this study. CMORPH shows the best performance among the SPPs, which generally all overestimate TSS, with a few exceptions. The seasonal analysis confirms that peaks of TSS are fairly well represented for both TMPA and CMORPH simulations.
- Simulated in-stream water temperature is well captured by all 3 SPP simulations with high correlations, low biases, and low RMSEs. While stream temperature is impacted by precipitation, and thus streamflow, it is most closely correlated to ambient air temperature and therefore presents the lowest variation and highest skills among all output variables evaluated in this study.
- Both DO and BOD show a large spatial variability among the 3 catchments in this study. Skills of all 3 SPPs are high for DO in the Upper Bull Run and Upper Broad Run catchments. However, a decreasing skill for each product is detected in the Cedar Run catchment. In comparison to streamflow and TSS, the variability in the DO metrics is notably smaller, indicating that precipitation has moderate impact on DO than on other water quality indicators evaluated in this analysis. Simulated DO concentrations for all 3 SPPs are fairly consistent with gauge-based simulations. Similar to gauge-based simulations, a strong flux in concentrations is seen in warmer months, which also overlaps with streamflow low-flow periods.
- The SPPs show satisfactory skills for BOD in the Upper Bull Run catchment, but low PCC in the Cedar Run and Upper Board Run catchments, especially when PERSIANN is used as input precipitation. The model performs well in terms of B and RMSE in the Upper Bull Run and Upper Board Run catchments, but has low skill in the Cedar Run catchment. Simulated BOD concentrations (mg/l) increase in warmer periods and drop during cooler periods following patterns associated with TW, yet this indicator also appears to be influenced by TSS concentrations during peak events.

Overall, results indicate that the spatiotemporal variability of the SPPs, along with the algorithms used by these products to estimate precipitation, have a quantifiable impact not only on streamflow, but also on water quality output from the hydrology model. However, it should be noted that there are limitations to this study. Foremost, this analysis was conducted in a single location, situated in the suburban Washington, D.C. area, characterized by a temperate climate and mild topographic variation. Additionally, this study only considered 1 hydrology/water quality model in this analysis, i.e., HSPF. While this model is well calibrated and has been validated to observation results, a different model may respond differently to changes in streamflow and water quality constituents resulting from forcing precipitation inputs. Nevertheless, this work represents a first attempt to utilize SPPs for water quality modeling, which could be of critical importance in areas of the world where rain-gauge networks or monitoring stations are either sparse or not available altogether. Future research should observe different regions and models, and other precipitation products such as re-analysis and blended products. Additionally, an in-depth analysis of the error propagation from the precipitation input to the water quality output could be performed to understand the performance from each SPPP to gauge-based data of the simulated water quality output from the HSPF hydrologic and water quality model. Multivariate statistical techniques could also be potentially applied to evaluate the seasonal and regional characteristics of watershed hydrology and additional water quality indicators by identifying spatial-temporal variations and trends in water quality at the watershed scale.

Funding

This research did not receive any specific grant from funding agencies in the public, commercial, or not-for-profit sectors.

Declaration of Competing Interest

None.

Acknowledgments, Samples, and Data

The authors would like to thank Editor-in-Chief Professor Denis Hughes and the 3 anonymous reviewers for their constructive comments and suggestions that improved the manuscript. The data used in this analysis are listed in the tables and supporting information files. The data sets necessary to reproduce the reported findings are publicly available from the archives. TRMM TMPA is available from: https://pmm.nasa.gov/data-access/downloads/TRMM. CMORPH is available from: ftp://ftp.cpc.ncep.noaa.gov/precip/global_CMORPH/30min_8km. PERSIANN is available from: ftp://persiann.eng.uci.edu/CHRSdata/PERSIANN−CCS/hrly/. The authors would like to thank Dr. Leonardo Porcacchia and Dr. Yiwen Mei who helped process the satellite precipitation data. The authors would also like to acknowledge financial support provided to the Occoquan Watershed Monitoring Laboratory from local jurisdictions and a local utility towards for both the Occoquan Watershed program and the Occoquan Model project.

Appendix A. Supplementary data

Supplementary material related to this article can be found, in the online version, at doi:https://doi.org/10.1016/j.ejrh.2019.100630.

References

Anagnostou, E.N., Maggioni, V., Nikolopoulos, E.I., Meskele, T., Hossain, F., Papadopoulos, A., 2010. Benchmarking high-resolution global satellite rainfall products to radar and rain-gauge rainfall estimates. IEEE Trans. Geosci. Remote. Sens. 48 (4), 1667–1683. https://doi.org/10.1109/TGRS.2009.2034736.

Azhar, S.C., Aris, A.Z., Yusoff, M.K., Ramli, M.F., Juahir, H., 2015. Classification of river water quality using multivariate analysis. Procedia Environ. Sci. 30, 79–84. https://doi.org/10.1016/j.proenv.2015.10.014.

Barakat, A., El Baghdadi, M., Rais, J., Aghezzaf, B., Slassi, M., 2016. Assessment of spatial and seasonal water quality variation of Oum Er Rbia River (Morocco) using multivariate statistical techniques. Int. Soil Water Conserv. Res. 4 (4), 284–292. https://doi.org/10.1016/j.iswcr.2016.11.002.

Bardossy, A., Das, T., 2008. Influence of rainfall observation network on model calibration and application. Hydrol. Earth Syst. Sci. Discuss. 13. https://doi.org/10.5194/hess-12-77-2008.

Beck, H.E., van Dijk, A.I.J.M., Levizzani, V., Schellekens, J., Miralles, D.G., Martens, B., de Roo, A., 2017. MSWEP: 3-hourly 0.25° global gridded precipitation (1979–2015) by merging gauge, satellite, and reanalysis data. Hydrol. Earth Syst. Sci. Discuss. 1–38. https://doi.org/10.5194/hess-2016-236.

Bengraïne, K., Marhaba, T.F., 2003. Using principal component analysis to monitor spatial and temporal changes in water quality. J. Hazard. Mater. 100 (1–3), 179–195. https://doi.org/10.1016/S0304-3894(03)00104-3.

Berrisford, P., Dee, D., Poli, P., Brugge, R., Fielding, K., Fuentes, M., et al., 2011. The ERA-Interim Archive, ERA Report Series No.1 Version 2.0. October Retrieved from. . http://www.ecmwf.int/publications/.

Bitew, M.M., Gebremichael, M., Ghebremichael, L.T., Bayissa, Y.A., 2012. Evaluation of high-resolution satellite rainfall products through streamflow simulation in a hydrological modeling of a small mountainous watershed in Ethiopia. J. Hydrometeorol. 13 (1), 338–350. https://doi.org/10.1175/2011JHM1292.1.

Bu, H., Tan, X., Li, S., Zhang, Q., 2010. Temporal and spatial variations of water quality in the Jinshui River of the South Qinling Mts., China. Ecotoxicol. Environ. Saf. 73 (5), 907–913. https://doi.org/10.1016/j.ecoenv.2009.11.007.

Chang, C.H., Cai, L.Y., Lin, T.F., Chung, C.L., van der Linden, L., Burch, M., 2015.). Assessment of the Impacts of Climate Change on the Water Quality of a Small Deep Reservoir in a Humid-Subtropical Climatic Region. Water 7 (12), 1687–1711. https://doi.org/10.3390/w7041687.

Chang, H., 2008. Spatial analysis of water quality trends in the Han River basin, South Korea. Water Res. 42 (13), 3285–3304. https://doi.org/10.1016/j.watres.2008.04.006.

Duda, P.B., Hummel, P.R., Donigian Jr., A.S., Imhoff, J.C., 2012. BASINS/HSPF: model use, calibration, and validation. Trans. Asabe 55 (4), 1523–1547. https://doi.org/10.13031/2013.42261.

Duque-Gardeazábal, N., Zamora, D., Rodríguez, E., 2018. Analysis of the Kernel Bandwidth Influence in the Double Smoothing Merging Algorithm to Improve Rainfall Fields in Poorly Gauged Basins. 635–626. https://doi.org/10.29007/2xp6.

Ebert, E.E., Janowiak, J.E., Kidd, C., 2007. Comparison of near-real-Time precipitation estimates from satellite observations and numerical models. Bull. Am. Meteorol. Soc. 88 (1), 47–64. https://doi.org/10.1175/BAMS-88-1-47.

Fovet, O., Humbert, G., Dupas, R., Gascuel-Odoux, C., Gruau, G., Jaffrezic, A., et al., 2018. Seasonal variability of stream water quality response to storm events captured using high-frequency and multi-parameter data. J. Hydrol. 559, 282–293. https://doi.org/10.1016/j.jhydrol.2018.02.040.

Gebregiorgis, A.S., Hossain, F., 2013. Understanding the dependence of satellite rainfall uncertainty on topography and climate for hydrologic model simulation. Ieee Trans. Geosci. Remote. Sens. 51 (1), 704–718. https://doi.org/10.1109/TGRS.2012.2196282.

Gelca, R., Hayhoe, K., Scott-Fleming, I., Crow, C., Dawson, D., Patiño, R., 2016. Climate-water quality relationships in Texas reservoirs: climate-water quality relationships in Texas reservoirs. Hydrol. Process. 30 (1), 12–29. https://doi.org/10.1002/hyp.10545.

Girons Lopez, M., Wennerström, H., Nordén, L., Seibert, J., 2015. Location and density of rain gauges for the estimation of spatial varying precipitation. Geogr. Ann. Ser. A Phys. Geogr. 97 (1), 167–179. https://doi.org/10.1111/geoa.12094.

Guo, H., Chen, S., Bao, A., Hu, J., Yang, B., Stepanian, P., 2015. Comprehensive evaluation of high-resolution satellite-based precipitation products over China. Atmosphere 7 (1), 6. https://doi.org/10.3390/atmos7010006.

Guo, R., Liu, Y., 2016. Evaluation of satellite precipitation products with rain gauge data at different scales: implications for hydrological applications. Water 8 (7), 281. https://doi.org/10.3390/w8070281.

Habib, E., ElSaadani, M., Haile, A.T., 2012a. Climatology-focused evaluation of CMORPH and TMPA satellite rainfall products over the Nile Basin. J. Appl. Meteorol. Climatol. 51 (12), 2105–2121. https://doi.org/10.1175/JAMC-D-11-0252.1.

Habib, E., Haile, A.T., Tian, Y., Joyce, R.J., 2012b. Evaluation of the high-resolution CMORPH satellite rainfall product using dense rain gauge observations and radar-based estimates. J. Hydrometeorol. 13 (6), 1784–1798. https://doi.org/10.1175/JHM-D-12-017.1.

Hema, N., Kant, K., 2017. Reconstructing missing hourly real-time precipitation data using a novel intermittent sliding window period technique for automatic

weather station data. J. Meteorol. Res. 31 (4), 774–790. https://doi.org/10.1007/s13351-017-6084-8.
Hong, Y., Gochis, D., Cheng, J., Hsu, K., Sorooshian, S., 2007. Evaluation of PERSIANN-CCS rainfall measurement using the NAME event rain gauge network. J. Hydrometeorol. 8 (3), 469–482. https://doi.org/10.1175/JHM574.1.
Hsu, K., Behrangi, A., Imam, B., Sorooshian, S., 2010. Extreme precipitation estimation using satellite-based PERSIANN-CCS algorithm. In: Gebremichael, M., Hossain, F. (Eds.), Satellite Rainfall Applications for Surface Hydrology. Springer, Dordrecht. https://doi.org/10.1007/978-90-481-2915-7_4.
Hsu, K., Gao, X., Sorooshian, S., Gupta, H.V., 1997. Precipitation estimation from remotely sensed information using artificial neural networks. J. Appl. Meteorol. 36 (9), 1176–1190. https://doi.org/10.1175/1520-0450(1997)036<1176:PEFRSI>2.0.CO;2.
Huffman, G.J., Bolvin, D.T., Nelkin, E.J., 2010. The TRMM multi-satellite precipitation analysis (TMPA). In: Gebremichael, M., Hossain, F. (Eds.), Satellite Rainfall Applications for Surface Hydrology. Springer, Dordrecht, pp. 3–22. https://doi.org/10.1007/978-90-481-2915-7_1.
Huffman, G.J., Bolvin, D.T., Nelkin, E.J., Wolff, D.B., Adler, R.F., Gu, G., et al., 2007. The TRMM Multisatellite Precipitation Analysis (TMPA): Quasi-Global, Multiyear, Combined-Sensor Precipitation Estimates at Fine Scales. J. Hydrometeorol. 8 (1), 38–55. https://doi.org/10.1175/JHM560.1.
Hussain, Y., Satgé, F., Hussain, M.B., Martinez-Carvajal, H., Bonnet, M.-P., Cárdenas-Soto, M., et al., 2018. Performance of CMORPH, TMPA, and PERSIANN rainfall datasets over plain, mountainous, and glacial regions of Pakistan. Theor. Appl. Climatol. 131 (3–4), 1119–1132. https://doi.org/10.1007/s00704-016-2027-z.
Jeznach, L.C., Hagemann, M., Park, M.H., Tobiason, J.E., 2017. Proactive modeling of water quality impacts of extreme precipitation events in a drinking water reservoir. J. Environ. Manage. 201, 241–251. https://doi.org/10.1016/j.jenvman.2017.06.047.
Johnson, T.E., Butcher, J.B., Parker, A., Weaver, C.P., 2012. Investigating the sensitivity of U.S. Streamflow and water quality to climate change: U.S. EPA global change research program's 20 watersheds project. J. Water Resour. Plan. Manag. 138 (5), 453–464. https://doi.org/10.1061/(ASCE)WR.1943-5452.0000175.
Joyce, R.J., Janowiak, J.E., Arkin, P.A., Xie, P., 2004. CMORPH: a method that produces global precipitation estimates from passive microwave and infrared data at high spatial and temporal resolution. J. Hydrometeorol. 5, 487–503. https://doi.org/10.1175/1525-7541(2004)005%3C0487:CAMTPG%3E2.0.CO;2.
Jung, K.Y., Lee, K.L., Im, T.H., Lee, I.J., Kim, S., Han, K.Y., Ahn, J.M., 2016. Evaluation of water quality for the Nakdong River watershed using multivariate analysis. Environ. Technol. Innov. 5, 67–82. https://doi.org/10.1016/j.eti.2015.12.001.
Kang, J.H., Lee, S.W., Cho, K.H., Ki, S.J., Cha, S.M., Kim, J.H., 2010. Linking land-use type and stream water quality using spatial data of fecal indicator bacteria and heavy metals in the Yeongsan river basin. Water Res. 44 (14), 4143–4157. https://doi.org/10.1016/j.watres.2010.05.009.
Kidd, C., Becker, A., Huffman, G.J., Muller, C.L., Joe, P., Skofronick-Jackson, G., Kirschbaum, D.B., 2017. So, How Much of the Earth's Surface is Covered by Rain Gauges? Bull. Am. Meteorol. Soc. 98 (1), 69–78. https://doi.org/10.1175/BAMS-D-14-00283.1.
Kim, J., Ryu, J.H., 2015. Quantifying a threshold of missing values for gap filling processes in daily precipitation series. Water Resour. Manag. 29 (11), 4173–4184. https://doi.org/10.1007/s11269-015-1052-5.
Kisi, O., Ay, M., 2014. Comparison of Mann–Kendall and innovative trend method for water quality parameters of the Kizilirmak River, Turkey. J. Hydrol. 513, 362–375. https://doi.org/10.1016/j.jhydrol.2014.03.005.
Lee, H., Kang, K., 2015. Interpolation of missing precipitation data using kernel estimations for hydrologic modeling. Adv. Meteorol. 2015, 1–12. https://doi.org/10.1155/2015/935868.
Li, J., Sorooshian, S., Higgins, W., Gao, X., Imam, B., Hsu, K., 2008. Influence of spatial resolution on diurnal variability during the north american monsoon. J. Clim. 21 (16), 3967–3988. https://doi.org/10.1175/2008JCLI2022.1.
Ma, Y., Yang, Y., Han, Z., Tang, G., Maguire, L., Chu, Z., Hong, Y., 2018. Comprehensive evaluation of ensemble multi-satellite precipitation dataset using the dynamic bayesian model averaging scheme over the tibetan plateau. J. Hydrol. 556, 634–644. https://doi.org/10.1016/j.jhydrol.2017.11.050.
Maggioni, V., Massari, C., 2018. On the performance of satellite precipitation products in riverine flood modeling: a review. J. Hydrol. 558, 214–224. https://doi.org/10.1016/j.jhydrol.2018.01.039.
Maggioni, V., Meyers, P.C., Robinson, M.D., 2016. A review of merged high-resolution satellite precipitation product accuracy during the tropical rainfall measuring mission (TRMM) era. J. Hydrometeorol. 00, 17. https://doi.org/10.1175/JHM-D-15-0190.1.
Maggioni, V., Nikolopoulos, E.I., Anagnostou, E.N., Borga, M., 2017. Modeling satellite precipitation errors over mountainous terrain: the influence of gauge density, seasonality, and temporal resolution. IEEE Trans. Geosci. Remote. Sens. 55 (7), 4130–4140. https://doi.org/10.1109/TGRS.2017.2688998.
Maggioni, V., Vergara, H.J., Anagnostou, E.N., Gourley, J.J., Hong, Y., Stampoulis, D., 2013. Investigating the applicability of error correction ensembles of satellite rainfall products in river flow simulations. J. Hydrometeorol. 14 (4), 1194–1211. https://doi.org/10.1175/JHM-D-12-074.1.
Maldonado, P.P., Moglen, G.E., 2012. Low-flow variations in source water supply for the Occoquan reservoir system based on a 100-year climate forecast. J. Hydrol. Eng. 18 (7), 787–796. https://doi.org/10.1061/(ASCE)HE.1943-5584.0000623.
McMillan, H., Jackson, B., Clark, M., Kavetski, D., Woods, R., 2011. Rainfall uncertainty in hydrological modelling: an evaluation of multiplicative error models. J. Hydrol. 400 (1–2), 83–94. https://doi.org/10.1016/j.jhydrol.2011.01.026.
Mei, K., Liao, L., Zhu, Y., Lu, P., Wang, Z., Dahlgren, R.A., Zhang, M., 2014a. Evaluation of spatial-temporal variations and trends in surface water quality across a rural-suburban-urban interface. Environ. Sci. Pollut. Res. - Int. 21 (13), 8036–8051. https://doi.org/10.1007/s11356-014-2716-z.
Mei, Y., Anagnostou, E.N., Nikolopoulos, E.I., Borga, M., 2014b. Error analysis of satellite precipitation products in mountainous basins. J. Hydrometeorol. 15 (5), 1778–1793. https://doi.org/10.1175/JHM-D-13-0194.1.
Mei, Y., Nikolopoulos, E.I., Anagnostou, E.N., Borga, M., 2016. Evaluating satellite precipitation error propagation in runoff simulations of mountainous basins. J. Hydrometeorol. 17 (5), 1407–1423. https://doi.org/10.1175/JHM-D-15-0081.1.
Milewski, A., Elkadiri, R., Durham, M., 2015. Assessment and comparison of TMPA satellite precipitation products in varying climatic and topographic regimes in Morocco. Remote Sens. 7 (5), 5697–5717. https://doi.org/10.3390/rs70505697.
Moulin, L., Gaume, E., Obled, C., Paris-Est, U., 2009. Uncertainties on mean areal precipitation: assessment and impact on streamflow simulations. Hydrol. Earth Syst. Sci. Discuss. 18.
Murdoch, P.S., Baron, J.S., Miller, T.L., 2000. Potential effects of climate change on surface-water quality in North America. J. Am. Water Resour. Assoc. 36 (2), 347–366. https://doi.org/10.1111/j.1752-1688.2000.tb04273.x.
Nijssen, B., Lettenmaier, D.P., 2004. Effect of precipitation sampling error on simulated hydrological fluxes and states: anticipating the Global Precipitation Measurement satellites. J. Geophys. Res. 109 (D2). https://doi.org/10.1029/2003JD003497.
Nóbrega, R.L.B., Lamparter, G., Hughes, H., Guzha, A.C., Amorim, R.S.S., Gerold, G., 2018. A multi-approach and multi-scale study on water quantity and quality changes in the Tapajós River basin, Amazon. Proc. Int. Assoc. Hydrol. Sci. 377, 3–7. https://doi.org/10.5194/piahs-377-3-2018.
Noori, R., Sabahi, M.S., Karbassi, A.R., Baghvand, A., Taati Zadeh, H., 2010. Multivariate statistical analysis of surface water quality based on correlations and variations in the data set. Desalination 260 (1–3), 129–136. https://doi.org/10.1016/j.desal.2010.04.053.
Porcacchia, L., Kirstetter, P.E., Gourley, J.J., Maggioni, V., Cheong, B.L., Anagnostou, M.N., 2017. Toward a polarimetric radar classification scheme for coalescence-dominant precipitation: application to complex terrain. J. Hydrometeorol. 18 (12), 3199–3215. https://doi.org/10.1175/JHM-D-17-0016.1.
Rasmussen, R., Baker, B., Kochendorfer, J., Meyers, T., Landolt, S., Fischer, A.P., et al., 2012. How well are we measuring snow: the NOAA/FAA/NCAR winter precipitation test bed. Bull. Am. Meteorol. Soc. 93 (6), 811–829. https://doi.org/10.1175/BAMS-D-11-00052.1.
Rienecker, M.M., Suarez, M.J., Gelaro, R., Todling, R., Bacmeister, J., Liu, E., et al., 2011. MERRA: NASA's modern-era retrospective analysis for research and applications. J. Clim. 24 (14), 3624–3648. https://doi.org/10.1175/JCLI-D-11-00015.1.
Roebber, P.J., 2009. Visualizing multiple measures of forecast quality. Weather. Forecast. 24 (2), 601–608. https://doi.org/10.1175/2008WAF2222159.1.
Schaefer, J.T., 1990. The critical success index as an Indicator of warning skill. Weather and Forecasing 570–575. https://doi.org/10.1175/1520-0434(1990)005%3C0570:TCSIAA%3E2.0.CO;2.
Seyyedi, H., Anagnostou, E.N., Beighley, E., McCollum, J., 2015. Hydrologic evaluation of satellite and reanalysis precipitation datasets over a mid-latitude basin. Atmos. Res. 164–165, 37–48. https://doi.org/10.1016/j.atmosres.2015.03.019.
Sharifi, E., Steinacker, R., Saghafian, B., 2018. Multi time-scale evaluation of high-resolution satellite-based precipitation products over northeast of Austria. Atmos. Res. 206, 46–63. https://doi.org/10.1016/j.atmosres.2018.02.020.
Soler, M., Regüés, D., Latron, J., Gallart, F., 2007. Frequency–magnitude relationships for precipitation, stream flow and sediment load events in a small Mediterranean

basin (Vallcebre basin, Eastern Pyrenees). CATENA 71 (1), 164–171. https://doi.org/10.1016/j.catena.2006.06.009.
Sorooshian, S., AghaKouchak, A., Arkin, P., Eylander, J., Foufoula-Georgiou, E., Harmon, R., et al., 2011. Advanced concepts on remote sensing of precipitation at multiple scales. Bull. Am. Meteorol. Soc. 92 (10), 1353–1357. https://doi.org/10.1175/2011BAMS3158.1.
Sorooshian, S., Hsu, K., Gao, X., Gupta, H.V., Imam, B., Braithwaite, D., 2000. Evaluation of PERSIANN System Satellite-Based Estimates of Tropical Rainfall. Bulletin of the American Meteorogogical Society 81 (9), 2035–2046. https://doi.org/10.1175/1520-0477(2000)081%3C2035:EOPSSE%3E2.3.CO;2.
Taylor, K.E., 2001. Summarizing multiple aspects of model performance in a single diagram. J. Geophys. Res. Atmos. 106 (D7), 7183–7192. https://doi.org/10.1029/2000JD900719.
Thorne, O., Fenner, R.A., 2011. The impact of climate change on reservoir water quality and water treatment plant operations: a UK case study: the impact of climate change on reservoir water quality and WTP operations. Water Environ. J. 25 (1), 74–87. https://doi.org/10.1111/j.1747-6593.2009.00194.x.
U.S. Environmental Protection Agency, 2000. *Meteorological Monitoring Guidance for Regulatory Modeling Applications* (Guidance Document No. EPA-454/R-99-005; p. 171). Retrieved from U.S. Environmental Protection Agency website. U.S. Environmental Protection Agency, Research Triangle Park, NC. https://www3.epa.gov/scram001/guidance/met/mmgrma.pdf.
Verdin, A., Funk, C., Rajagopalan, B., Kleiber, W., 2016. Kriging and local polynomial methods for blending satellite-derived and gauge precipitation estimates to support hydrologic early warning systems. IEEE Trans. Geosci. Remote. Sens. 54 (5), 2552–2562. https://doi.org/10.1109/TGRS.2015.2502956.
Villarini, G., Smith, J.A., Serinaldi, F., Ntelekos, A.A., 2011. Analyses of seasonal and annual maximum daily discharge records for central Europe. J. Hydrol. 399 (3–4), 299–312. https://doi.org/10.1016/j.jhydrol.2011.01.007.
von Freyberg, J., Studer, B., Kirchner, J.W., 2017. A lab in the field: high-frequency analysis of water quality and stable isotopes in stream water and precipitation. Hydrol. Earth Syst. Sci. 21 (3), 1721–1739. https://doi.org/10.5194/hess-21-1721-2017.
Wang, L., Wang, Y., Xu, C., An, Z., Wang, S., 2011. Analysis and evaluation of the source of heavy metals in water of the River Changjiang. Environ. Monit. Assess. 173 (1–4), 301–313. https://doi.org/10.1007/s10661-010-1388-5.
Wunderlin, D.A., Valeria, A.M.A., Fabiana, P.S., Cecilia, H.A., 2001. Pattern Recognition Techniques for the Evaluation of Spatial and Temporal Variations in Water Quality. A Case Study: Suquía River Basin (Córdoba–Argentina). Water Res. 35 (12), 2881–2894. https://doi.org/10.1016/S0043-1354(00)00592-3.
Xie, P., Joyce, R., Wu, S., Yoo, S.-H., Yarosh, Y., Sun, F., Lin, R., 2017. Reprocessed, Bias-Corrected CMORPH Global High-Resolution Precipitation Estimates from 1998. J. Hydrometeorol. 18 (6), 1617–1641. https://doi.org/10.1175/JHM-D-16-0168.1.
Xu, H.S., Xu, Z.X., Wu, W., Tang, F.F., 2012. Assessment and Spatiotemporal Variation Analysis of Water Quality in the Zhangweinan River Basin, China. Procedia Environ. Sci. 13, 1641–1652. https://doi.org/10.1016/j.proenv.2012.01.157.
Xu, X., Li, J., Tolson, B.A., 2014. Progress in integrating remote sensing data and hydrologic modeling. Prog. Phys. Geogr. 38 (4), 464–498. https://doi.org/10.1177/0309133314536583.
Xu, Z., 2005. A Complex, Linked Watershed-Reservoir Hydrology and Water Quality Model Application for the Occoquan Watershed, Virginia (Dissertation). Retrieved from. Virginia Polytechnic Institute and State University. https://vtechworks.lib.vt.edu/bitstream/handle/10919/37186/dissertation_zhongyan.pdf.
Xu, Z., Godrej, A.N., Grizzard, T.J., 2007. The hydrological calibration and validation of a complexly-linked watershed–reservoir model for the Occoquan watershed, Virginia. J. Hydrol. 345 (3–4), 167–183. https://doi.org/10.1016/j.jhydrol.2007.07.015.
Yang, Y., Luo, Y., 2014. Evaluating the performance of remote sensing precipitation products CMORPH, PERSIANN, and TMPA, in the arid region of northwest China. Theor. Appl. Climatol. 118 (3), 429–445. https://doi.org/10.1007/s00704-013-1072-0.
Zeng, Q., Chen, H., Xu, C.-Y., Jie, M.-X., Chen, J., Guo, S.-L., Liu, J., 2018. The effect of rain gauge density and distribution on runoff simulation using a lumped hydrological modelling approach. J. Hydrol. 563, 106–122. https://doi.org/10.1016/j.jhydrol.2018.05.058.